

DEUTSCHES ELEKTRONEN-SYNCHROTRON

DESY

DESY 65/5  
Juni 1965  
Experimente

PHOTOPRODUCTION OF MESONS IN A HYDROGEN

BUBBLE CHAMBER AT ENERGIES UP TO 5.5 GEV

U. Brall, G. Reimann

I. Physikalisches Institut der Technischen Hochschule, Aachen,

K. Lanius, A. Meyer and A. Pose

Forschungsstelle für Physik hoher Energien der Deutschen Akademie  
der Wissenschaften zu Berlin-Zeuthen.

J. Moebes, W. Tejessy

Physikalisches Institut der Universität Bonn

D. Cords, G. Knies, E. Lohrmann, H. Meyer, G. Wolf, DESY, Hamburg

D. Lüke, D. Pollmann, E. Raubold, H. Spitzer, P. Söding  
Physikalisches Staatsinstitut, II. Institut für Experimental-  
physik, Hamburg

H. Beisel, E. Burkhardt, H. Filthuth, H. Kolar, P. Steffen  
Institut für Hochenergiephysik der Universität Heidelberg

P. Freund, P. Seyboth, J. Seyerlein

Max-Planck-Institut für Physik und Astrophysik, München

and

R. Florent, G. Harigel, G. Horlitz, G. Kessler, G. Linser,  
R.I. Louttit, M.W. Teucher (French-German Bubble Chamber  
Collaboration)

PHOTOPRODUCTION OF MESONS IN A HYDROGEN  
BUBBLE CHAMBER AT ENERGIES UP TO 5.5 GEV

U. Brall, G. Reimann,  
I. Physikalisches Institut der Technischen Hochschule, Aachen.

K. Lanius, A. Meyer and A. Pose,  
Forschungsstelle für Physik hoher Energien der Deutschen Akademie  
der Wissenschaften zu Berlin-Zeuthen.

J. Moebes, W. Tejessy,  
Physikalisches Institut der Universität Bonn.

D. Cords, G. Knies, E. Lohrmann, H. Meyer, G. Wolf,  
DESY, Hamburg

D. Lüke, D. Pollmann, E. Raubold, H. Spitzer, P. Söding,  
Physikalisches Staatsinstitut, II. Institut für Experimentalphysik, Hamburg

H. Beisel, E. Burkhardt, H. Filthuth, H. Kolar, P. Steffen  
Institut für Hochenergiephysik der Universität Heidelberg

P. Freund, P. Seyboth, J. Seyerlein  
Max-Planck-Institut für Physik und Astrophysik, München

and

R. Florent<sup>\*</sup>, G. Harigel<sup>†</sup>, G. Horlitz<sup>†</sup>, G. Kessler<sup>†</sup>, G. Linser<sup>†</sup>,  
R. I. Louttit<sup>\*\*</sup>, M. W. Teucher<sup>†</sup> (French-German Bubble Chamber-  
Collaboration)

---

<sup>\*</sup> CEA Saclay

<sup>†</sup> DESY, Hamburg

<sup>\*\*</sup> Brookhaven National Lab.

Introduction:

An experiment to study photoproduction of mesons on protons was started at DESY by passing a bremsstrahlung beam through a hydrogen bubble chamber. Up to now about 400 000 pictures have been taken. We report here first results from part of this film. Most of our results agree with similar work from CEA<sup>1)</sup> and with more recent and more accurate CEA data<sup>2)</sup>.

Experimental Procedure:

The layout of the experiment is shown in fig. 1. The  $\gamma$ -ray beam from the electron synchrotron hits an external target upstream of QB1 and produces a secondary positron beam with a momentum of 5.5 GeV/c. This beam hits a second target between MB2 and MB3. The bremsstrahlung from this target passes through a LiH beam hardener of 0.6 radiation units thickness (in the first part of the run 0.8 r.u. were used), and then through the 80 cm hydrogen bubble chamber. Details of the chamber will be published later. Some of the main data are: Sensitive volume 40 x 40 x 80 cm<sup>3</sup>, three cameras, magnetic field about 22 kGauss, repetition rate 1/sec for this run.

All film was scanned twice and the events were measured and processed by our standard geometry and kinematics (GRIND) programs. Separation of the various hypotheses was made by the  $X^2$  value of the fit and by ionization measurements on the tracks. For the events with three outgoing charged particles (three prong events), the only reaction giving a 3-constraint-fit is  $\gamma p \rightarrow p\pi^+\pi^-$ , because here all kinematical variables except the energy of the photon are known. (The direction of the incident beam was known with an accuracy of better than 3 mrad). Identification of this reaction was made by ionization and by demanding  $X^2 \leq 14$ . The mean value of  $X^2$  was 2.8.

All other reactions with  $\leq 3$  charged particles and without strange particles have 0 constraints. This means, that they can be kinematically determined (including the primary photon energy) only if an assumption is made about the effective mass of the unobserved neutral particles. These reactions were separated by ionization measurements and by kinematics with assumed mass values for the neutral particles. We assumed the smallest mass compatible with the reaction, i.e.  $\pi^0$  or neutron mass.

Table 1 gives the number of events measured:

Table 1:

reaction	number of events	% of film used
$\gamma p \rightarrow p\pi^0(\pi^0 \dots)$	388	32
$n\pi^+(\pi^0 \dots)$	354	32
$p\pi^+\pi^-$	547	100
$p\pi^+\pi^-\pi^0(\pi^0 \dots)$	226	100
$n\pi^+\pi^+\pi^-(\pi^0 \dots)$	101	100
5 prong events	41	100
strange particles	22	59
undecidable	29	100
sum	1708	

For the one prong events ( $\gamma p \rightarrow p\pi^0(\pi^0 \dots)$  and  $n\pi^+(\pi^0 \dots)$ ) only film with a small density of background tracks was used.

Cross sections: The flux and energy spectrum of the photons was determined by measuring electron positron pairs in the chamber (see fig. 2).

Fig. 3 shows the cross sections for the various reactions as a function of the primary photon energy. Fig. 4 and 5 show the energy distribution of events with one outgoing charged particle, assuming that they are of the type  $\gamma p \longrightarrow p\pi^0$  and  $n\pi^+$ . Generally more  $\pi^0$  mesons can of course be produced. In this case the assumption made above will lead to an underestimate of the photon energy. Fig. 4 and 5 show that the great majority of events lie in the region of the  $3/2, 3/2$   $\pi$ -nucleon resonance. The solid line represents the number of events expected from single pion production alone. It is derived from counter measurements up to 1 GeV. The agreement is quite satisfactory. The cross section of the counter measurements for single pion production is also added to the total cross section for 3-prong and 5-prong events in fig. 2. This gives a lower limit for the total cross section around 1 GeV. In order to get limits for the total cross section at high energies, one has first to estimate the contribution of the one prong events. We assumed that all one prong events which are not accounted for by the single pion production cross section between 0.15 GeV and 1 GeV, have an energy  $> 1$  GeV. This will overestimate the contribution of one prong events at high energies, since some of the events should come from multiple pion production below 1 GeV and should thus not be included. We assumed further that the cross section for these events is constant between 1 GeV and 5.5 GeV. This will probably also overestimate the contribution at the highest energy since one expects from statistical model calculations that the percentage of one prong events drops for higher energies. One gets in this way an upper limit for the contribution of the one prong events to the total  $\gamma p$  cross section at 5 GeV.

A second correction is due to the fact that we cannot distinguish events with one neutral particle from events with more than one

neutral particle. Since we fitted the events with the assumption that not more than one neutral particle is present, the primary energy will be underestimated for events with more than one neutral particle. We have used the cross section for five prong events and the branching ratios from the statistical model to obtain an estimate for the cross section of three prong events with more than one neutral particle. At 4-5 GeV it amounts to  $30 \mu\text{b}$ . This contribution together with the upper limit from the one prong events is included in fig. 3 at 4.7 GeV. One would conclude from the upper and the lower limits in fig. 3 that the total  $\gamma\text{p}$  cross section at 5 GeV is smaller than at 1 GeV.

The cross sections given for strange particle production are corrected for events decaying in the charged mode outside the chamber and for neutral decays.

#### Production of resonances:

We observe the production of the  $3/2 \ 3/2 \ \pi\text{N}$  resonance and the  $\rho$ -meson in the reaction  $\gamma\text{p} \longrightarrow \text{p}\pi^+\pi^-$  and the  $\omega$ -meson in the reaction  $\gamma\text{p} \longrightarrow \text{p}\pi^+\pi^-\pi^0$ . Production of the  $\text{N}_{33}^*$  isobar and of the  $\rho$ -meson accounts for a large fraction of the total cross section of the reaction  $\gamma\text{p} \longrightarrow \text{p}\pi^+\pi^-$ . Production of the  $\omega$ -meson is significantly smaller than  $\rho$ -production. Fig. 6 - 8 show the corresponding distributions of the effective masses for several ranges of the primary photon energy.

We used two methods to estimate the production cross sections of the resonances. With the first method we determined the number of events in the mass region of the resonance, which lie above a background predicted by phase space. The phase space was averaged with

the photon energy spectrum over the range of photon energies considered. For the second method the data are fitted by the sum of the phase space distribution plus a Breit Wigner distribution for the resonance ("B.W. fit" in table II). This method gives probably a better estimate for the true cross section. For the  $\omega$ -meson a normal distribution was used for the fit. For photon energies from 1.1 GeV to 1.8 GeV both the  $\rho$ -meson and the  $N_{33}^*$  were observed and were therefore simultaneously fitted by Breit-Wigner distributions. The  $\rho$  mass distribution is shifted towards lower mass values compared with the accepted value of the  $\rho$  mass. In contrast, the mass of the  $\omega$  meson agreed with the expected value.

The  $N_{33}^*$  production cross section from the reaction  $\gamma p \rightarrow N_{33}^{*++} \pi^-$  has a maximum around 1 GeV and drops sharply for energies above 1 GeV. The  $\rho$  and  $\omega$  production cross sections appear to decrease slowly with energy. Table II summarizes the results.

Table II: Cross sections in  $\mu b$

	$.6 < E_\gamma < 1.1 \text{ GeV}$	$1.1 < E_\gamma < 1.8 \text{ GeV}$	$1.8 < E_\gamma < 5.5 \text{ GeV}$
$\rho$ -meson production: B.W. fit $ t  < .3 \text{ GeV}^2$		$20 + 5$ $\left\{ \begin{array}{l} 10.5 + 3.2 \\ \text{above backg.} \end{array} \right.$	$14 + 3$ $\left\{ \begin{array}{l} 6.3 + 2.0 \\ \text{above backg.} \end{array} \right.$
$\omega$ -meson production: total $ t  < .3 \text{ GeV}^2$		$7.6 + 2.1$ $\sim 1.3$	$5.3 + 1.3$ $\sim 2$
$N_{33}^*$ -production:  B.W. fit $ t  < .3 \text{ GeV}^2$ (B.W. fit)	$\sim 56$ $\sim 46$	$15 + 5$ $\sim 9$	$\lesssim 6$ $\underline{\quad}$
theoretical prediction ( $ t  < .3 \text{ GeV}^2$ )	44	18	5

x) not including neutral decay.

The peripheral  $\rho$ -production can be compared with the predictions of the one pion exchange model. Therefore, the cross section for small absolute values of  $t$ , the four momentum transfer squared between initial and final proton is given in table II. Calculations with absorptive corrections were made by Jackson<sup>3)</sup> and by Schilling<sup>4)</sup>. The theoretical cross sections were integrated over the proper range of photon energies, using values for the absorption parameters of  $C = 0.8$  and  $A = 9.6 \text{ GeV}^{-2}$ .

$C$  is connected with the opacity and  $A$  with the slope of the elastic diffraction peak of  $\rho$ -p-scattering. According to these calculations the cross section for  $|t| < .3 \text{ GeV}^2$  decreases by a factor of 3.3, if the photon energy increases from the range  $1.1 \text{ GeV} < E_\gamma < 1.8 \text{ GeV}$  to the range  $1.8 \text{ GeV} < E_\gamma < 5.5 \text{ GeV}$ . The experimentally observed value for this ratio is  $1.7 \pm .7$ . Another check is given by the angular distribution of the  $\rho$ -decay. The one pion exchange model without absorption predicts a  $\sin^2\theta$  distribution, where  $\theta$  is the angle between the direction of the photon and the  $\pi^-$  meson from  $\rho$ -decay in the  $\rho$  rest system. The  $\sin^2\theta$  distribution is modified by absorption effects, as calculated by Jackson and Schilling. Our experimental distribution for  $|t| < .3 \text{ GeV}^2$  is in disagreement with a  $\sin^2\theta$  distribution. This is shown in fig. 9. It is, however, also inconsistent with the theoretical distribution modified by absorption effects. Fig. 9 shows also the experimental distribution of the four momentum transfer squared. The theoretical prediction with the values of the absorption parameters given above is compatible with the experimental data.



In order to get some insight into the  $N^*$  production by the reaction  $\gamma p \rightarrow N_{3,3}^{x++} \pi^-$ , we compared the data with the one pion exchange predictions of the Drell effect.<sup>5)</sup> We applied the theory for small absolute values of  $t$ , the square of the four momentum transfer between incident photon and final  $\pi^-$  ( $|t| < .3 \text{ GeV}^2$ ). Stichel and Scholz<sup>6)</sup> gave an improved theory for this process, which is gauge invariant. We avoided the high energy approximation of Drell's formula, which is sometimes used and applied the exact expression<sup>7)</sup> (see appendix), since most of the isobar production is around 1 GeV. The resulting values are shown in table 2. For photon energies between 0.6 GeV and 1.1 GeV there is a fair agreement with the experimental value. For higher energies the experimental cross section seems to drop somewhat faster than the theoretical prediction.

#### Acknowledgements:

We are greatly indebted to the machine group of DESY for all their efforts and for the excellent performance of the synchrotron, and to the operating crews of the bubble chamber, the hydrogen liquifier and the beam line. We also thank our scanners for their painstaking work. The work in the laboratories in Aachen, Bonn, Hamburg (II. Institut für Experimentalphysik), Heidelberg and München was supported by the Bundesministerium für wissenschaftliche Forschung.

Figure Captions:

Fig. 1 - Experimental arrangement

T : target

QB, QD: quadrupole magnets

MB, MA: bending magnets

Z: counter

K : collimator

BS: beam shutter

Qu: quantameter

BH: beam hardener

Fig. 2 - Photon energy spectrum. Beam hardener 0.8 r.u. without magnetic field. The full line represents a theoretical thin target bremsstrahlung spectrum.

Fig. 3 - Total cross sections. The estimate for upper and lower limits for cross sections, see text. The cross sections were determined with the assumption that not more than one neutral outgoing particle is present.

Fig. 4 - Energy spectrum of events with single outgoing proton. For calculating the photon energy, a reaction of the type  $\gamma p \rightarrow p\pi^0$  was assumed. The full line shows the prediction for the number of events expected from counter measurements for the reaction  $\gamma p \rightarrow p\pi^0$ .

Fig. 5 - Energy spectrum of events with a single outgoing  $\pi^+$  meson. For calculating the photon energy, a reaction of the type  $\gamma p \rightarrow n\pi^+$  was assumed. The full line shows the prediction for the number of events expected from counter measurements for the reaction  $\gamma p \rightarrow n\pi^+$ .

References:

- 1.) - H. R. Crouch et al., Phys. Rev. Lett., 13, 636, 640 (1964),
- 2.) - H.R. Crouch et al., International Symposium on Electron and Photon Interactions at High Energies, Hamburg 1965.
- 3.) - J. D. Jackson, private communication
- 4.) - K. Schilling, International Symposium on Electron and Photon Interactions at High Energies, Hamburg, 1965
- 5.) - S. D. Drell, Phys. Rev. Lett., 5, 278 (1960)
- 6.) - P. Stichel and M. Scholz, Nuovo Cim., 34, 1381 (1964)
- 7.) - P. Stichel, private communication.

Fig. 6 - Mass distribution of the  $\pi^+ \pi^-$  combination from the reaction  
 $\gamma p \longrightarrow p \pi^+ \pi^-$ .

Fig. 7 - Mass distribution of the  $\pi^+ \pi^- \pi^0$  combination from the reaction  
 $\gamma p \longrightarrow p \pi^+ \pi^- \pi^0 (\pi^0 \dots)$ .

Fig. 8 - Mass distribution of the  $p \pi^+$  combination from the reaction  
 $\gamma p \longrightarrow p \pi^+ \pi^-$ .

Fig. 9 - Top: Distribution of the square of the four momentum transfer  $t$  between incident and outgoing proton for the reaction  $\gamma p \rightarrow p \rho^0$ . Background is subtracted and an average over photon energies from 1.1 GeV to 5.5 GeV is taken. The full line is the prediction of the one pion exchange model with absorption corrections.

Bottom: Angular distribution of the  $\pi^-$  from  $\rho$ -decay with respect to the direction of the incident photon, in the  $\rho$  rest system, for events with  $|t| < .3 \text{ GeV}^2$ . Full line:  $\sin^2 \theta$  distribution expected for one pion exchange without absorption. Dotted line: calculated<sup>4)</sup> using the absorption model with  $C = 1$ ,  $A = 9.3 \text{ GeV}^{-2}$ .

Appendix:

Differential cross section of isobar production in the reaction  $\gamma p \rightarrow N_{3,3}^{x++} \pi^-$ , according to Stichel <sup>7)</sup>, in the overall center of mass system.

$$\frac{d^3\sigma}{dq_0 d\Omega} = \frac{1}{137} \cdot \frac{1}{2\pi^2} \cdot \frac{|p|^{-1} \sqrt{s'} |q|}{\sqrt{s} |k|} \cdot \sigma_{33}(s')$$

$$\cdot \left\{ \frac{|q|^2 \sin^2\theta |p|^2}{(t - \mu^2)^2} + \frac{1}{2} + \frac{25}{64} \left[ \frac{(p_2 \cdot q)^2}{s'} - \mu^2 \right] \frac{|q|^2 \sin^2\theta}{(p_2 \cdot k)^2} \right.$$

$$+ \frac{5}{4} \frac{|q|^2 \sin^2\theta}{(t - \mu^2)(p_2 \cdot k)} \left[ \frac{1}{2}(t + \mu^2) + \frac{1}{2} \frac{(p_2 \cdot q)}{s'} (s' + t - M^2) \right]$$

$$\left. - \frac{5}{8} \cdot \frac{|q|^2 \sin^2\theta}{(p_2 \cdot k)} \cdot \left[ \frac{(p_2 \cdot q)}{s'} + 1 \right] \right\}$$

where  $(p_2 \cdot k) = -1/2 (M^2 + \mu^2 - s - t)$

$(p_2 \cdot q) = 1/2 (s - \mu^2 - s')$

$k$  is the four-vector of the incident photon,  $p_1$  denotes the four vector of the incident proton,  $p_2$  and  $q$  the outgoing  $N^{x++}$  resp.  $\pi^-$  meson.

$s = (k + p_1)^2$ ,  $t = (k - q)^2$ ,  $\mu$  = pion mass,  $M$  = proton mass,  $s' = (k + p_1 - q)^2$ ,  $|p|^2 = (s' - M^2 + \mu^2)/4s' - \mu^2$ ,  $|q|$  = three momentum,  $q_0$  = total energy of  $\pi^-$ ,  $\sigma_{33}(s') = \pi^+ - p$  cross section at square of center of mass energy  $s'$  of the  $p - \pi^+$  system.

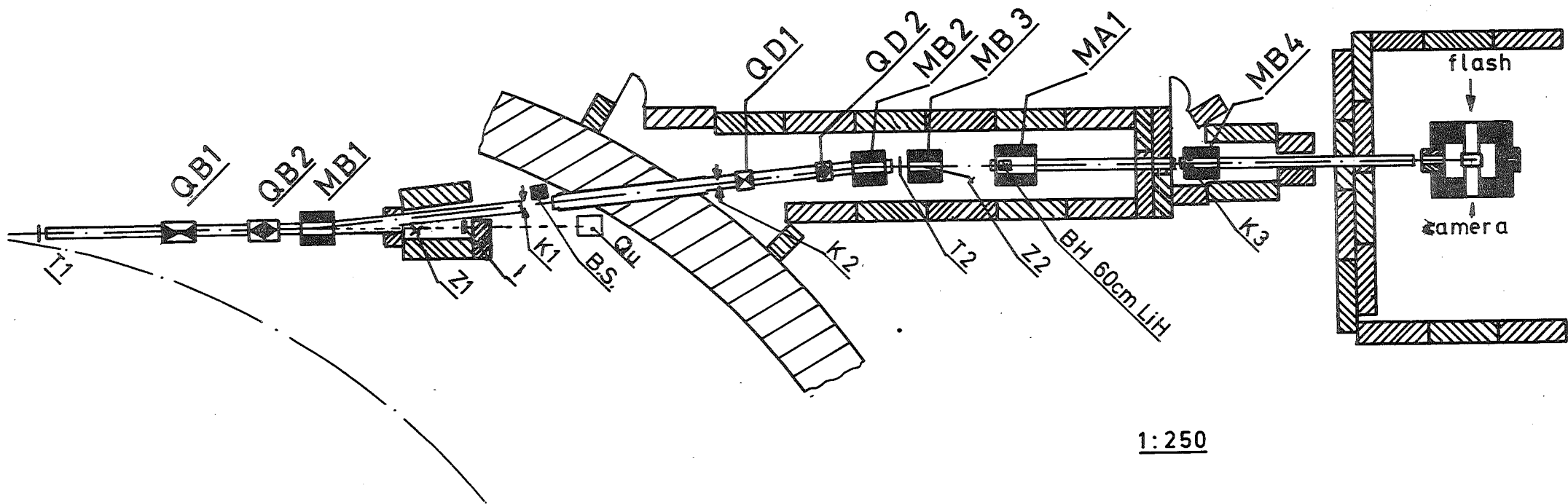


FIG. 1

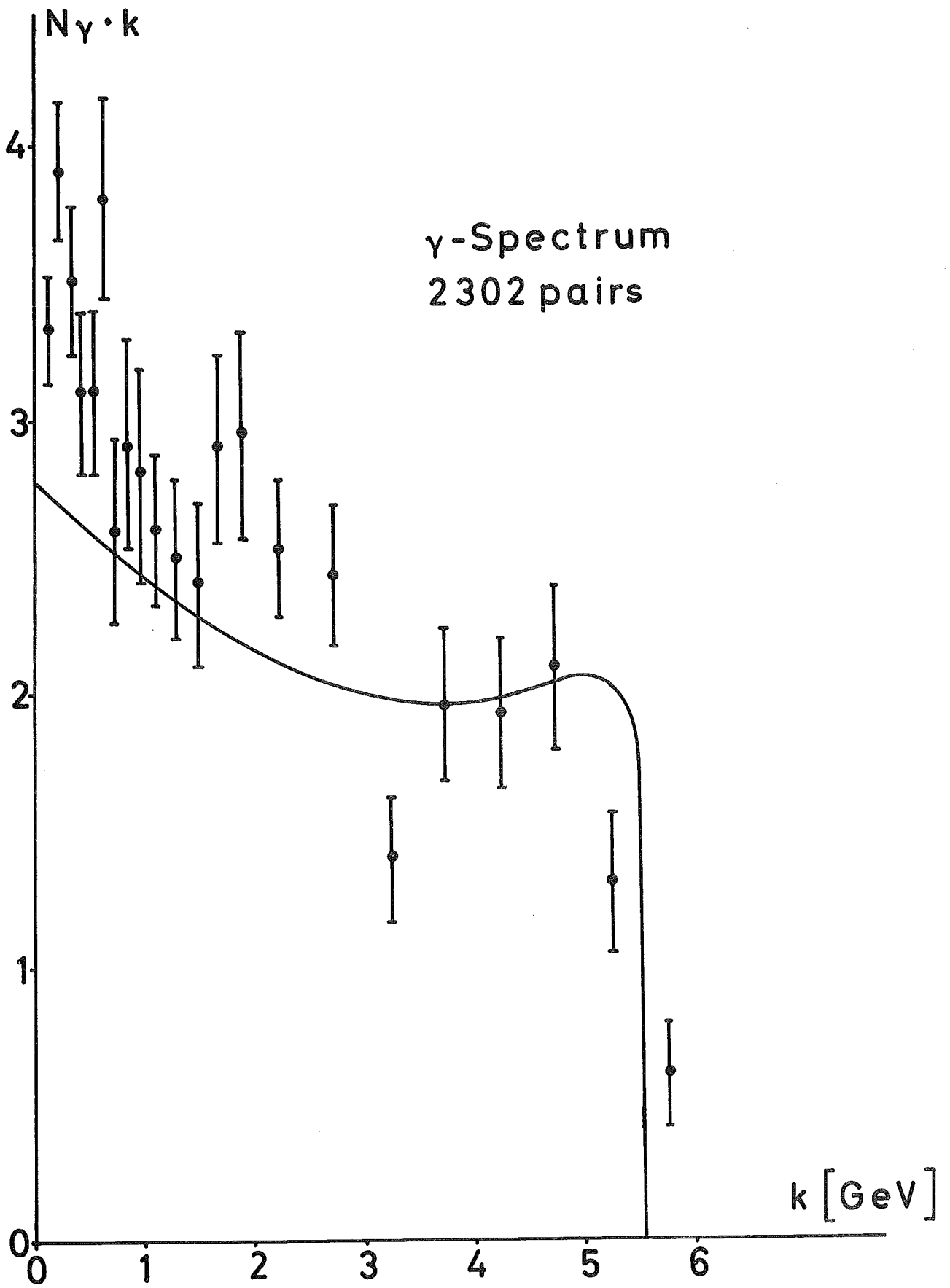


FIG. 2

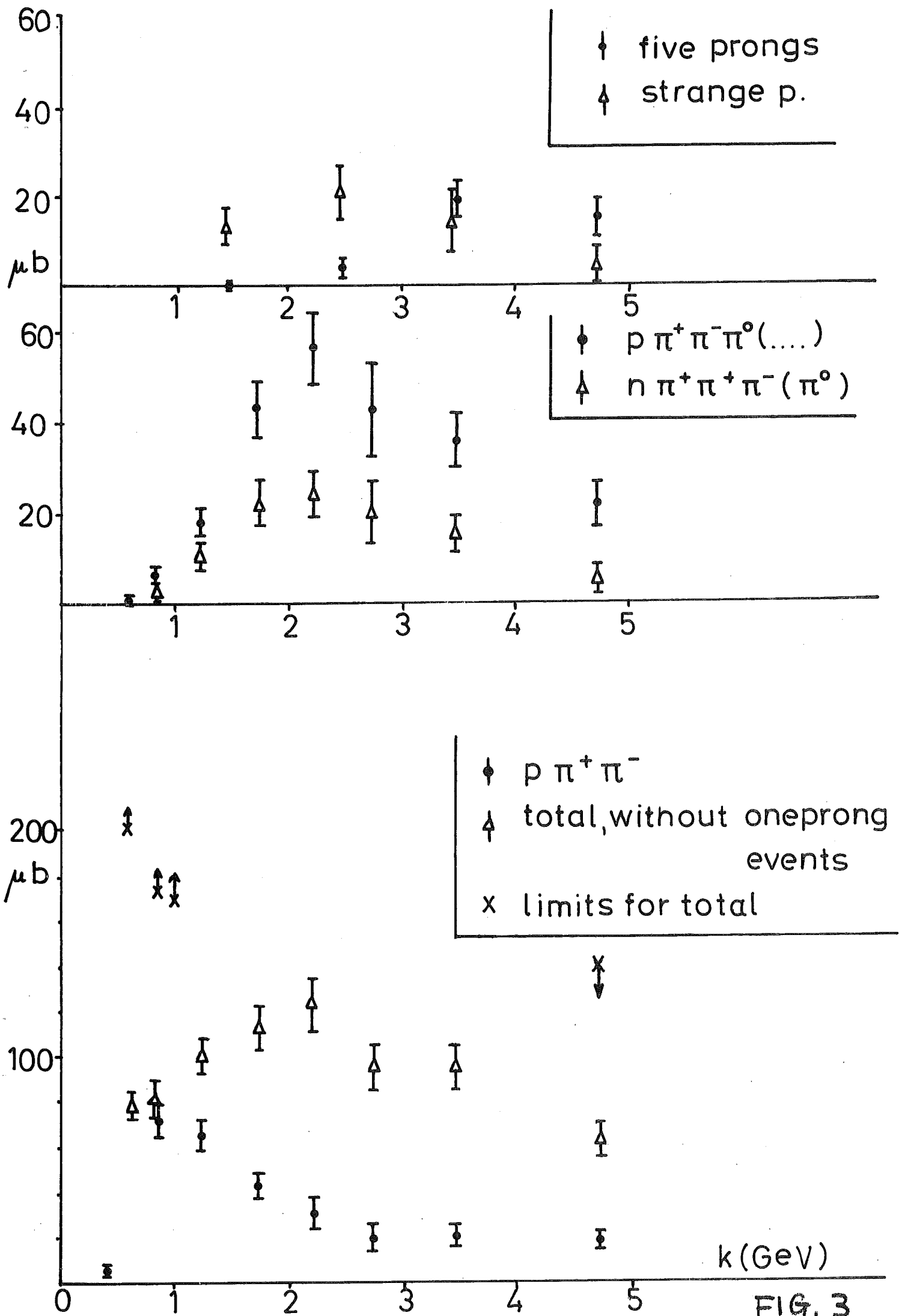
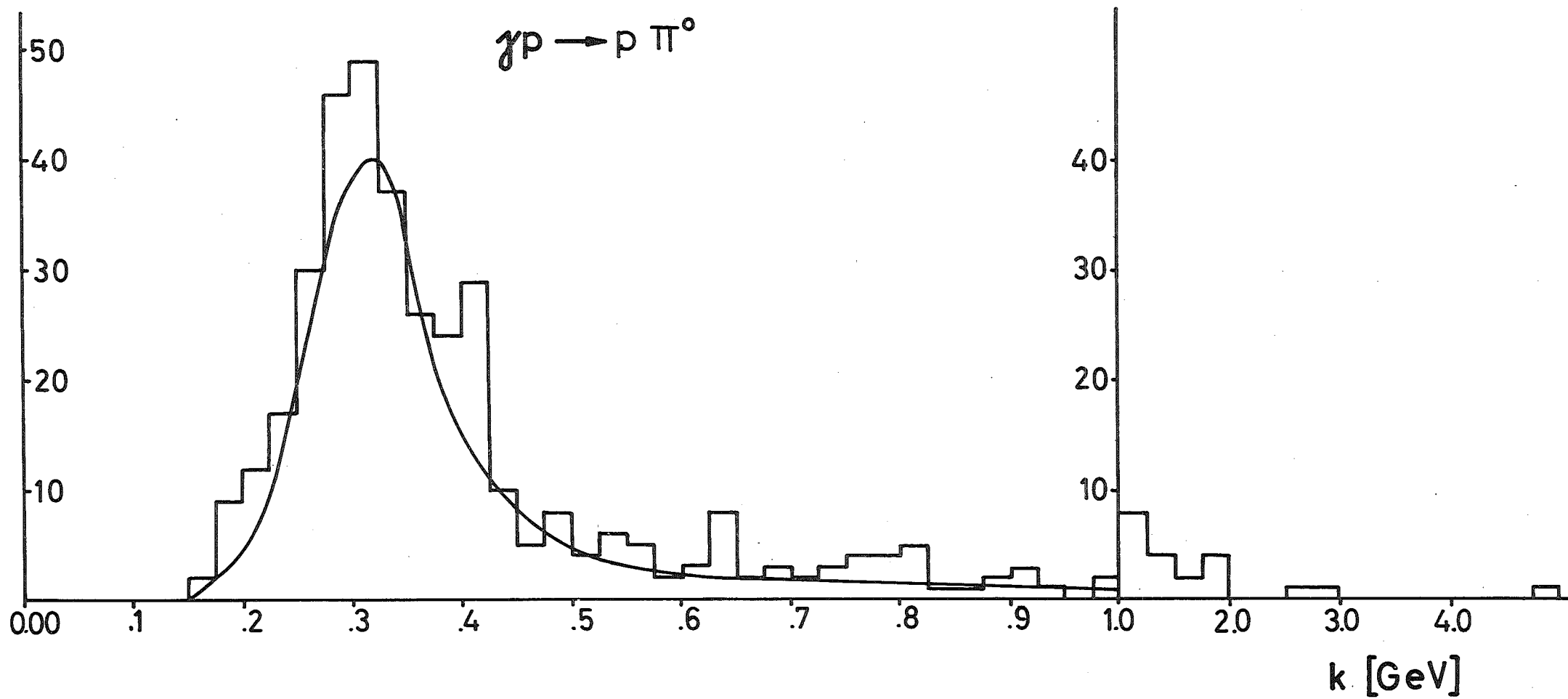


FIG. 3





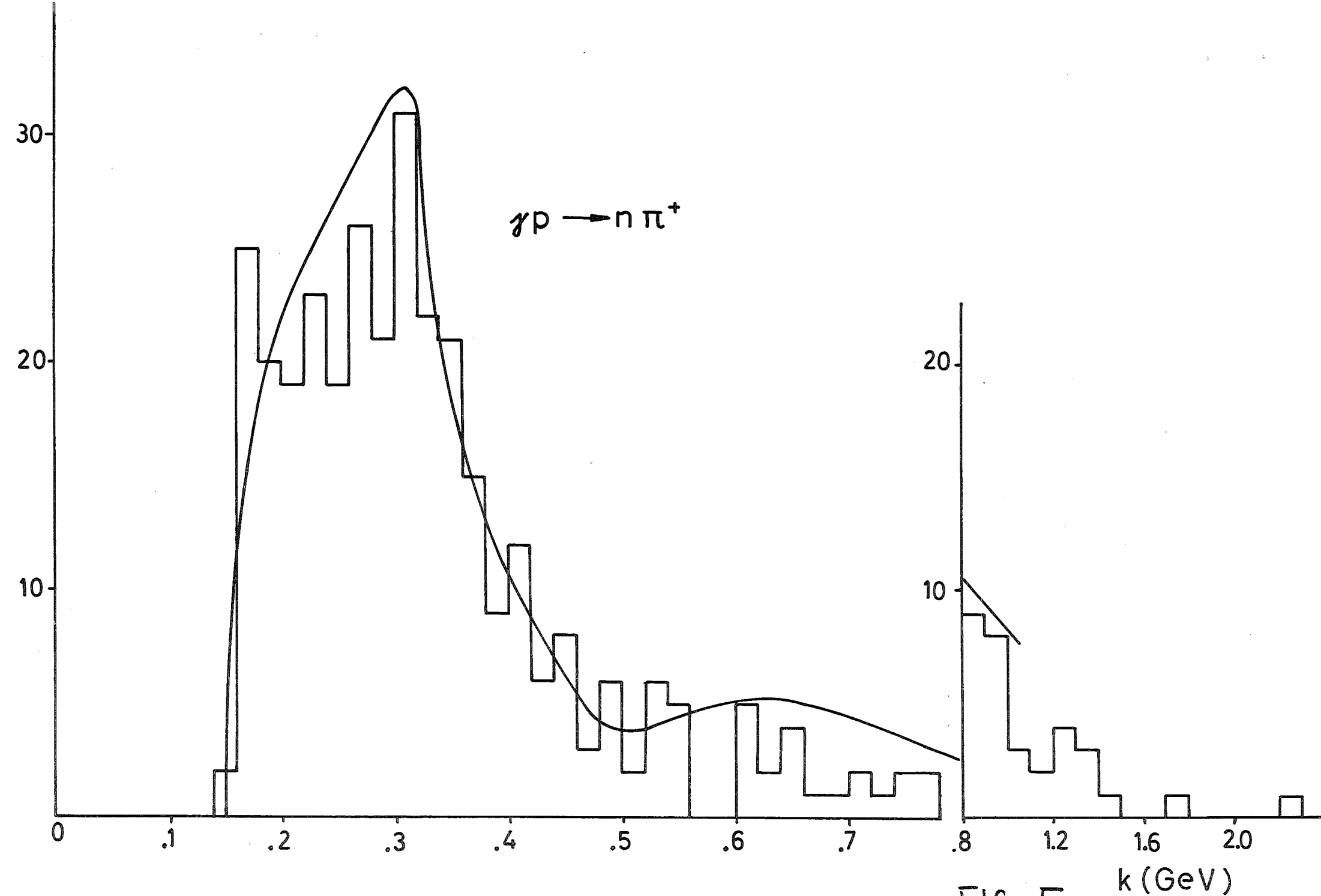


FIG. 5 k (GeV)

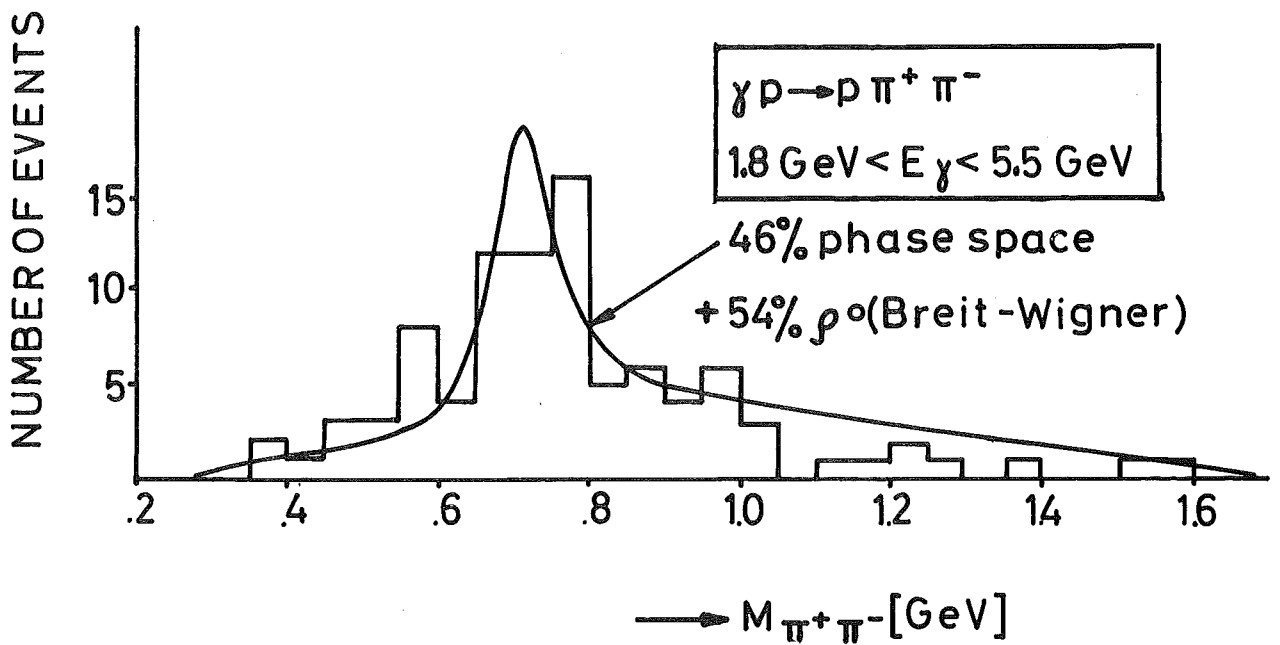
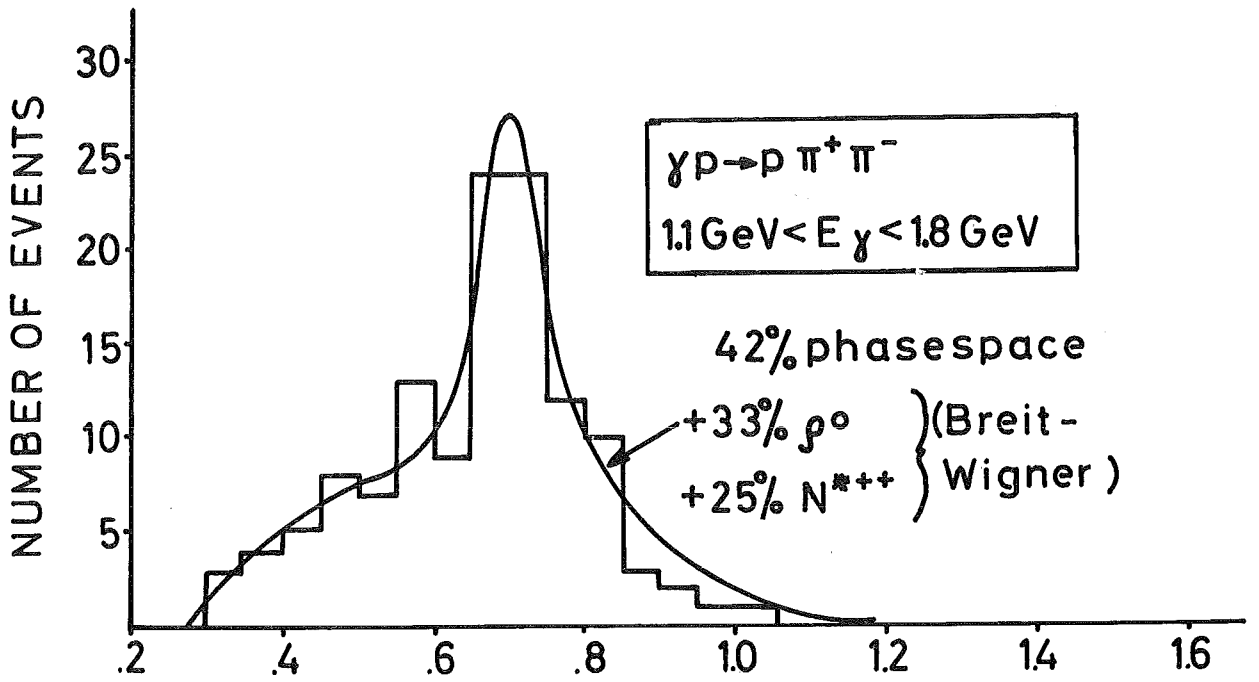


FIG. 6

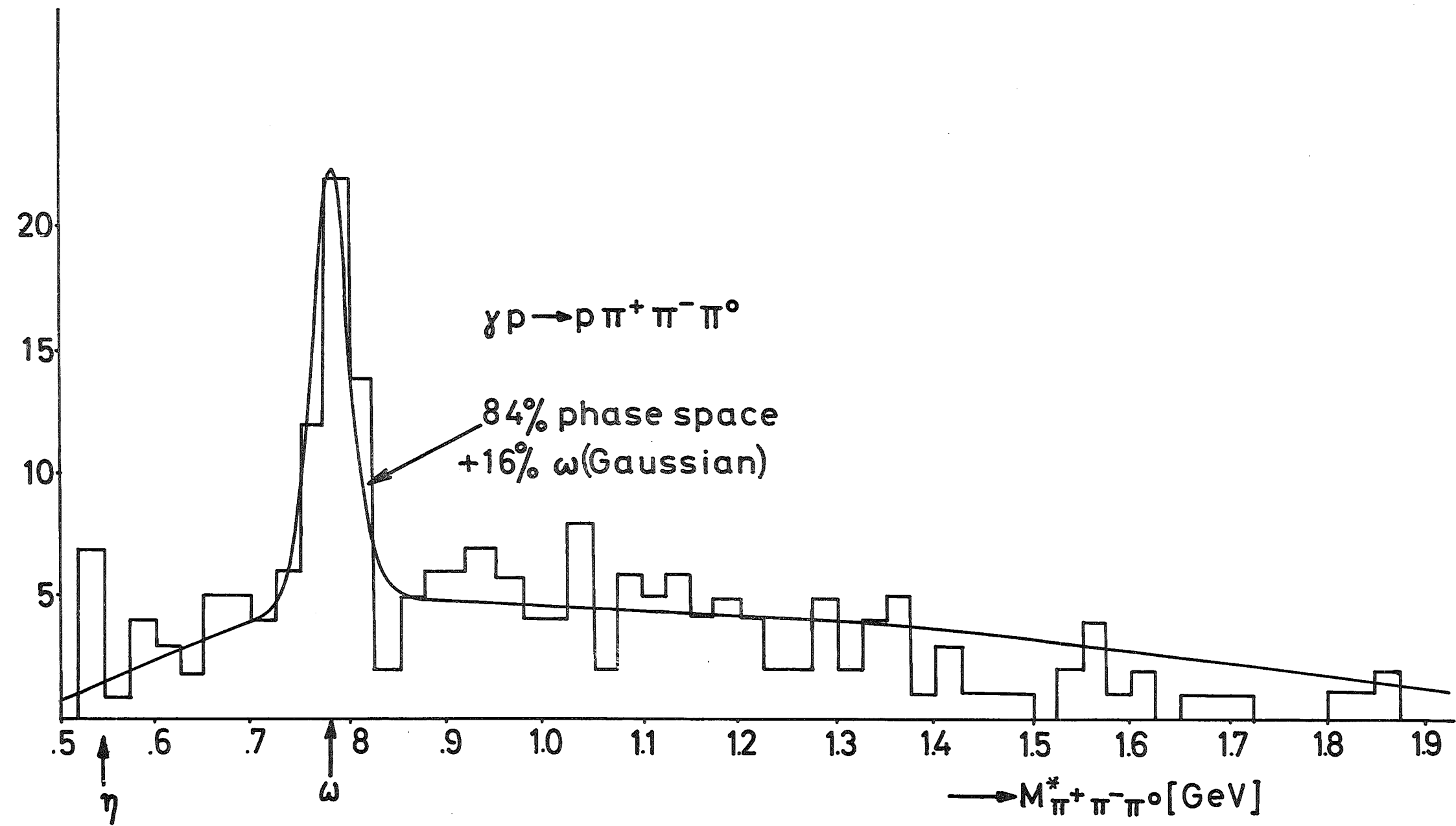


FIG.7

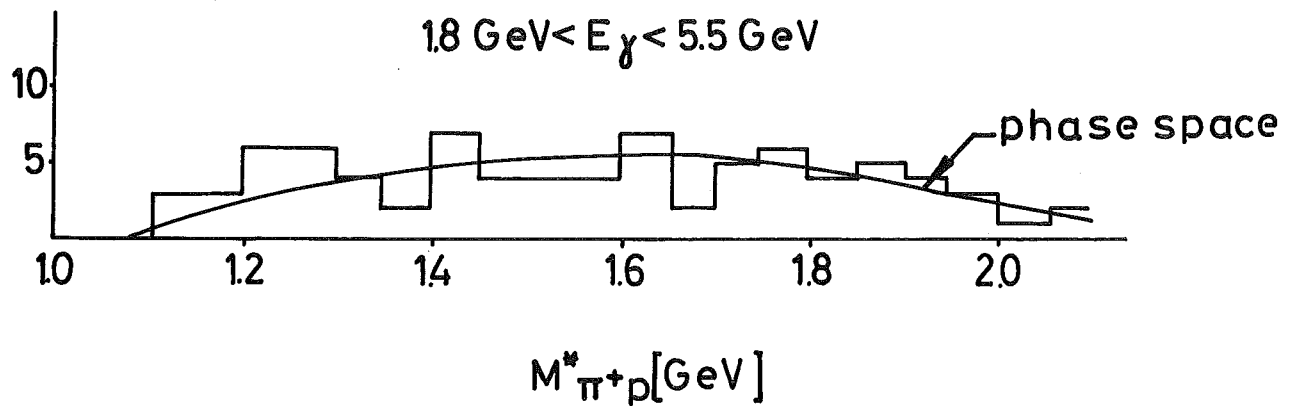
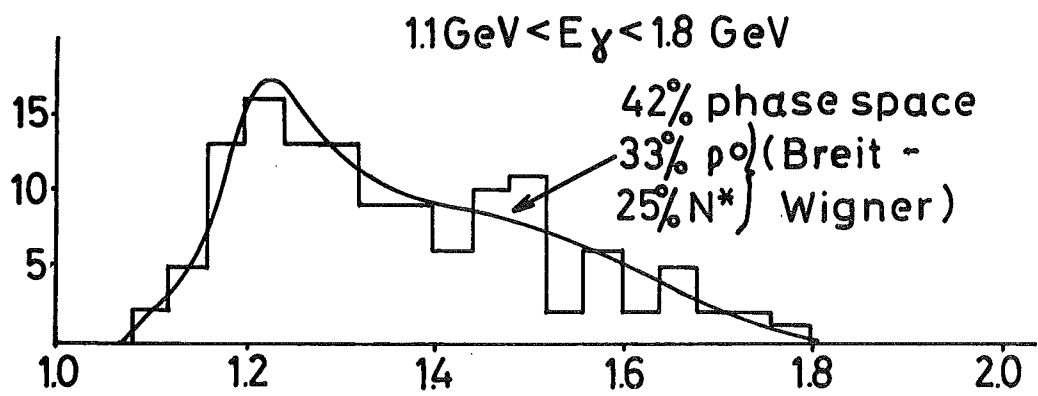
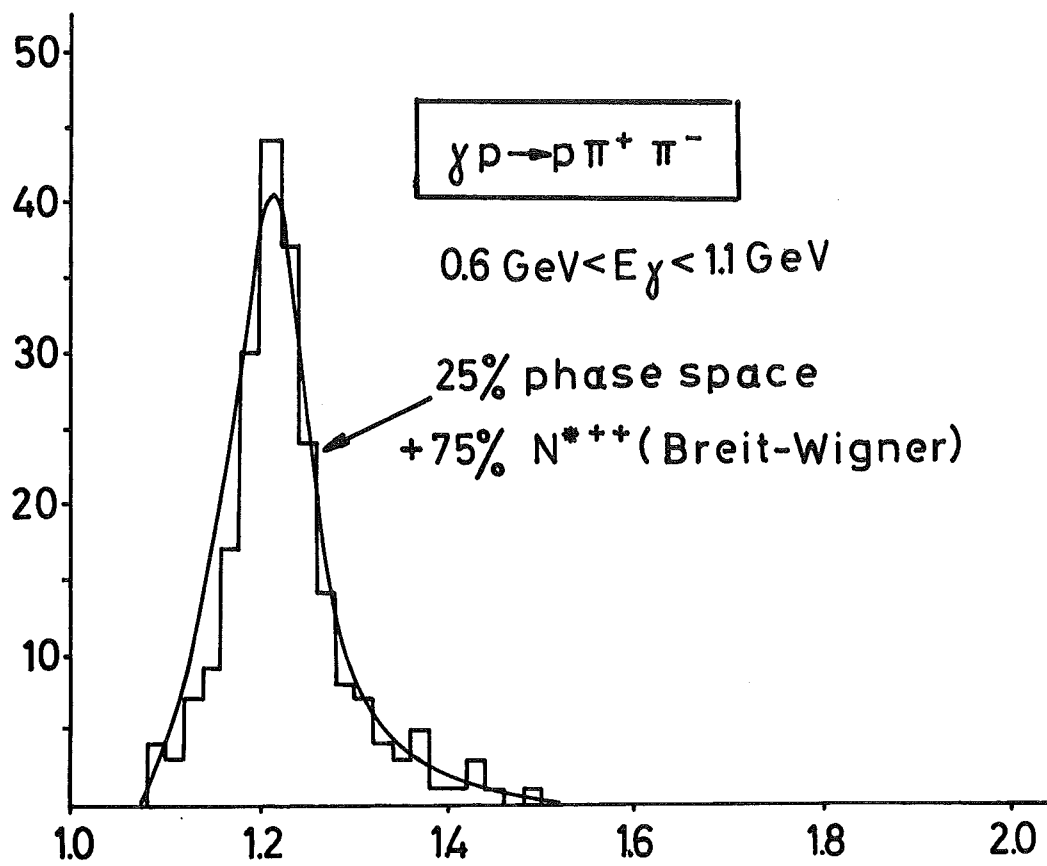


FIG. 8

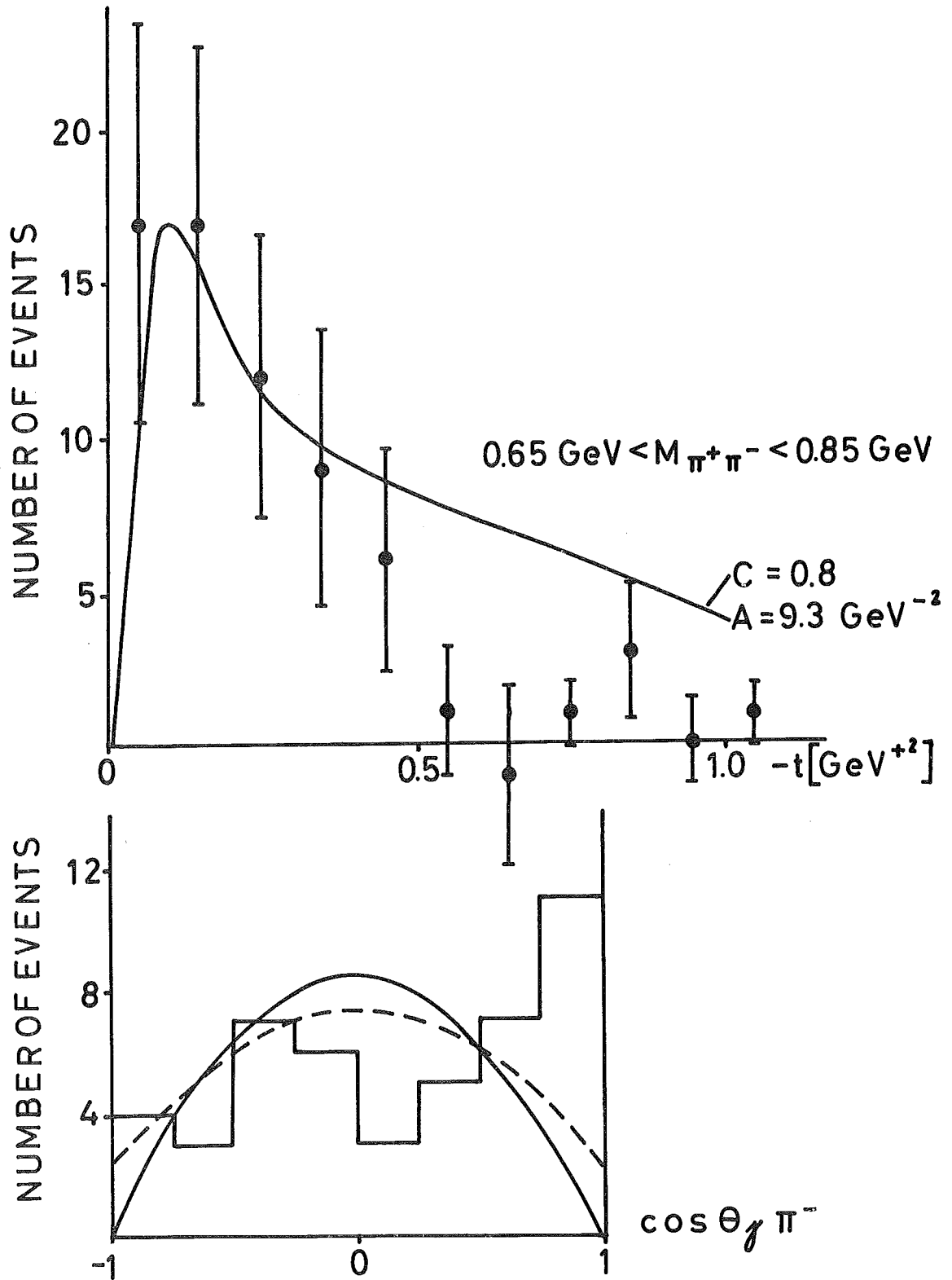


FIG. 9